ARL 72-0007
JANUARY 1972

Aerospace Research Laboratories

APPLICATION OF RADIOGRAPHIC TECHNIQUES TO STUDIES OF PARTICLE LADEN FLOW

B. N. TURMAN, 1stLT, USAF
ENERGY CONVERSION RESEARCH LABORATORY

RICHARD E. PERRAULT
SYSTEMS RESEARCH LABORATORY
DAYTON, OHIO

PROJECT NO. 7116

Approved for public release; distribution unlimited.

AIR FORCE SYSTEMS COMMAND
United States Air Force

NOTICES

When Government drawings, specifications, or other data are used for any purpose other than in connection with a definitely related Government procurement operation, the United States Government thereby incurs no responsibility nor any obligation whatsoever; and the fact that the Government may have formulated, furnished, or in any way supplied the said drawings, specifications, or other data, is not to be regarded by implication or otherwise as in any manner licensing the holder or any other person or corporation, or conveying any rights or permission to manufacture, use, or sell any patented invention that may in any way be related thereto.

Agencies of the Department of Defense, qualified contractors and other government agencies may obtain copies from the

Defense Documentation Center
Cameron Station
Alexandria, Virginia 22314

This document has been released to the

CLEARINGHOUSE
U. S. Department of Commerce
Springfield, Virginia 22151

for the sale to the public.

Copies of ARL Technical Documentary Reports should not be returned to Aerospace Research Laboratories unless return is required by security considerations, contractual obligations or notices on a specified document.

AIR FORCE: 12-4-72/300

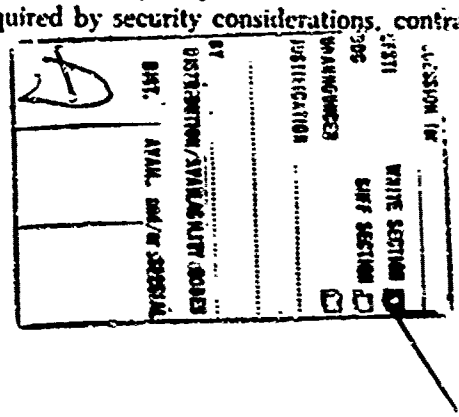

UNCLASSIFIED
Security Classification

DOCUMENT CONTROL DATA - R & D

(Security classification of title, body of abstract and indexing annotation must be entered when the overall report is classified)

1 ORIGINATING ACTIVITY (Corporate author)	2a. REPORT SECURITY CLASSIFICATION
Energy Conversion Research Laboratory Aerospace Research Laboratories Wright-Patterson Air Force Base, Ohio 45433	UNCLASSIFIED 2b. GROUP

3 REPORT TITLE

"Application of Radiographic Techniques to Studies of Particle Laden Flow"

4 DESCRIPTIVE NOTES (Type of report and inclusive dates)

Scientific Final

5 AUTHOR(S) (First name, middle initial, last name)

Lt Bobby N. Turman
Richard E. Perrault

6. REPORT DATE	7a. TOTAL NO OF PAGES	7b. NO. OF REFS
January 1972	46	17

8a. CONTRACT OR GRANT NO	9a. ORIGINATOR'S REPORT NUMBER(S)
b. PROJECT NO. 7116-00-03	
c. DoD Element 61102F	9b. OTHER REPORT NO(S) (Any other numbers that may be assigned this report)
d. DoD Subelement 681308	ARL 72-0007

10 DISTRIBUTION STATEMENT

Approved for public release; distribution unlimited.

11 SUPPLEMENTARY NOTES	12. SPONSORING MILITARY ACTIVITY
TECH OTHER	Aerospace Research Laboratories(LE) Wright-Patterson AFB, Ohio 45433

13. ABSTRACT

Attenuation of X-radiation is used to measure powder density in flowing systems. This report describes the experimental absorption and procedures utilized to make such measurements. A discussion is given of the effect of the X-ray intensity spectrum on the effective absorption coefficient of the powder. An error analysis is presented, and maximum and minimum density measurements for the experiment are calculated. The absorption experiment gives the value of powder density, ρ, multiplied by absorption path length, ℓ. Because of experimental errors, the minimum value of this product which can be determined is $\rho\ell$ = 0.03 gm/cm^2 (for talc powder), while the maximum value is $\rho\ell$ = 9. gm/cm^2. Radiographs, density contours, and radial density profiles from multicomponent vortex flow experiments are presented.

DD FORM 1 NOV 68 1473

UNCLASSIFIED
Security Classification

14. KEY WORDS	LINK A		LINK B		LINK C	
	ROLE	WT	ROLE	WT	ROLE	WT
X-rays						
Multicomponent Flow						
Flow Diagnostics						

*U.S.Government Printing Office: 1972 — 759-084/436

ARL 72-0007

APPLICATION OF RADIOGRAPHIC TECHNIQUES TO STUDIES OF PARTICLE LADEN FLOW

B. N. TURMAN
ENERGY CONVERSION RESEARCH LABORATORY

AND

RICHARD E. PERRAULT
SYSTEMS RESEARCH LABORATORY

JANUARY 1972

PROJECT 7116

AEROSPACE RESEARCH LABORATORIES
AIR FORCE SYSTEMS COMMAND
UNITED STATES AIR FORCE
WRIGHT-PATTERSON AIR FORCE BASE, OHIO

FOREWORD

The radiographic techniques described in this report were developed for measurements of powder density distributions in multi-component vortex flow. This work is part of the multi-component flow research program conducted by the Energy Conversion Research Laboratory, under Project No. 7116.

The authors wish to thank the following people for their assistance, advice, and consultation during the course of this work: Lt James M. Howard, Mr. Siegfried Hasinger, and Dr. Hans J.P. VonOhain, of Aerospace Research Laboratories, and Mr. Jack Watson, Mr. Brian Hausfeld, and Dr. Ronald Versic of Systems Research Laboratories.

ABSTRACT

Attenuation of X-radiation is used to measure powder density in flowing systems. This report describes the experimental absorption and procedures utilized to make such measurements. A discussion is given of the effect of the X-ray intensity spectrum on the effective absorption coefficient of the powder. An error analysis is presented, and maximum and minimum density measurements for the experiment are calculated. The absorption experiment gives the value of powder density, ρ, multiplied by absorption path length, ℓ. Because of experimental errors, the minimum value of this product which can be determined is $\rho\ell \approx 0.03$ gm/cm^2 (for talc powder), while the maximum value is $\rho\ell = 9.$ gm/cm^2. Radiographs, density contours, and radial density profiles from multicomponent vortex flow experiments are presented.

TABLE OF CONTENTS

LIST OF FIGURES

I. INTRODUCTION

For a number of years, the Energy Conversion Laboratory has been engaged in the study of multi-phase, multi-component flows, with principal applications in the areas of dust separation devices and high power density energy sources. One of the many variables to be measured in these experiments is particle concentration within the flow, and several techniques have been proposed to measure this quantity. One possible technique would employ a tube inside the flow, with a suitable extraction and monitoring system to measure the density of particles at a given location. This method suffers limitations at large particle density because of the tendency of the powder to plug the probe, as well as having the problem of flow disturbances produced by the probe. Another method of measuring particle density in the flow is to observe attenuation of a beam of light passing through the flow. This method is good for a limited range of particle concentration, but becomes completely useless at large particle density. A fiber-optics probe could be devised to alleviate this problem (by using a shorter absorption path length), but the use of a probe inside the flow field would still present disturbance problems. An alternate solution to this problem would be to use radiation which is not absorbed as readily by the particle material. For example, the light beam could be replaced by an X-ray beam, thus increasing the maximum measurable powder density. Through extensive experimentation, we have shown that this X-ray absorption technique is an effective method of measuring particle concentration in the high density range of interest here.

The X-ray absorption technique has been used previously in a number of fluid dynamic experiments. Absorption of soft X-rays (about 4 kv. energy) was used to study density profiles in supersonic gas flow (Reference 1); detonation waves in combustible gases were studied through X-ray absorption (Reference 2); and shock waves in water were analyzed from soft X-ray photography (Reference 3). Rowe and Partridge (References 4, 5) showed that relatively hard X-rays (about 100 kv. energy) were effective for photographing the bubbling process in fluidized beds. In order to provide the sharp time resolution required to get distinct images of rising gas bubbles in the bed, and to take sequential exposures to determine bubble velocities, an intensifying screen and high speed movie camera were used to record X-ray transmission. Very good qualitative data was obtained: sharp images of air bubbles in the bed were shown, and eddy currents, particle diffusion, and mixing were clearly observable. This method has been widely used to observe bubbling and slugging phenomena in fluidized beds (References 6, 7). Absorption of low energy X-rays has been used in an automatic system for determining particle size distributions by sedimentation (Reference 8).

The purpose of this report is to show the utility of the X-ray absorption method for quantitative measurements of powder density in multi-component flows. The general experimental technique will be described, as well as expected errors. Representative data from several experiments will be presented to illustrate the results obtained with this technique.

II. EXPERIMENTAL EQUIPMENT

A schematic drawing of the X-ray system is shown in Figure 1. The radiation source was a General Electric Model 100-15 Medical X-ray unit, designed for general medical and dental X-ray diagnosis. Operating voltage was variable from 40 - 100 kvp, with regulated tube current of either 10 or 15 ma: typically the unit was operated at 100 kvp and 15 ma. The X-ray tube was self-rectifying, meaning that output radiation followed a 60 cps, half-wave rectified curve. Focal spot for the tube was 1.5 mm in diameter. Exposure time could be varied from 1/60 sec to 5 sec: although this unit was not designed for high precision work, exposure time variations were found to be less than 1%. A variable iris diaphragm was provided to limit the X-ray field of view to the minimum required for a given exposure, thus reducing stray scattering from peripheral apparatus. This scattering problem was further reduced by the use of a lead mask placed directly over the subject area. Kodak Industrial X-ray film, type AA-2, was used to record X-ray intensity transmitted through the subject flow. 4" x 5" sheet film, prepackaged in lighttight paper envelope, was clamped in position on a plexiglas film holder, as shown in Figure 1. Considerable back scatter was observed with this arrangement, but the problem was eliminated by placing a 1/16" thick lead sheet behind the film.

To protect personnel from hazardous stray radiation, the X-ray tube, film, and flow experiment were all situated inside a lead-lined box. In order to house vortex chambers with diameters of some 36 inches and lengths

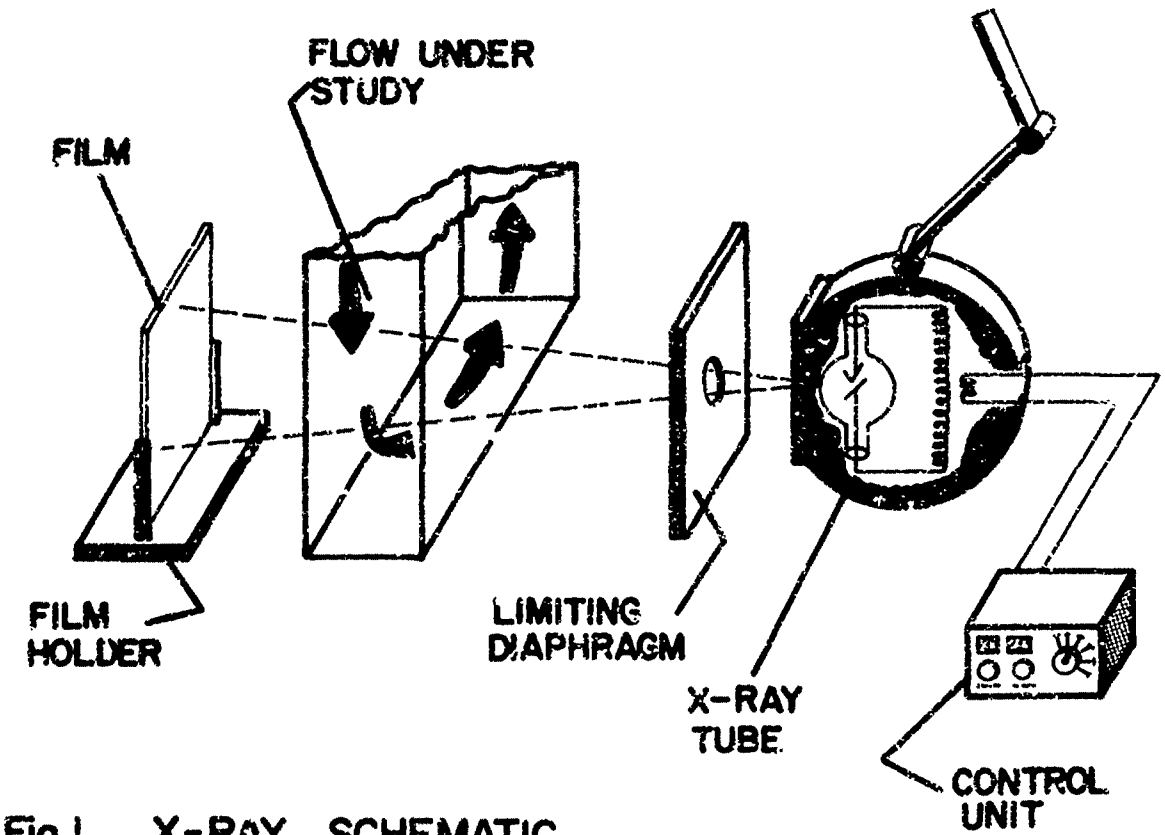

Fig.1 X-RAY SCHEMATIC

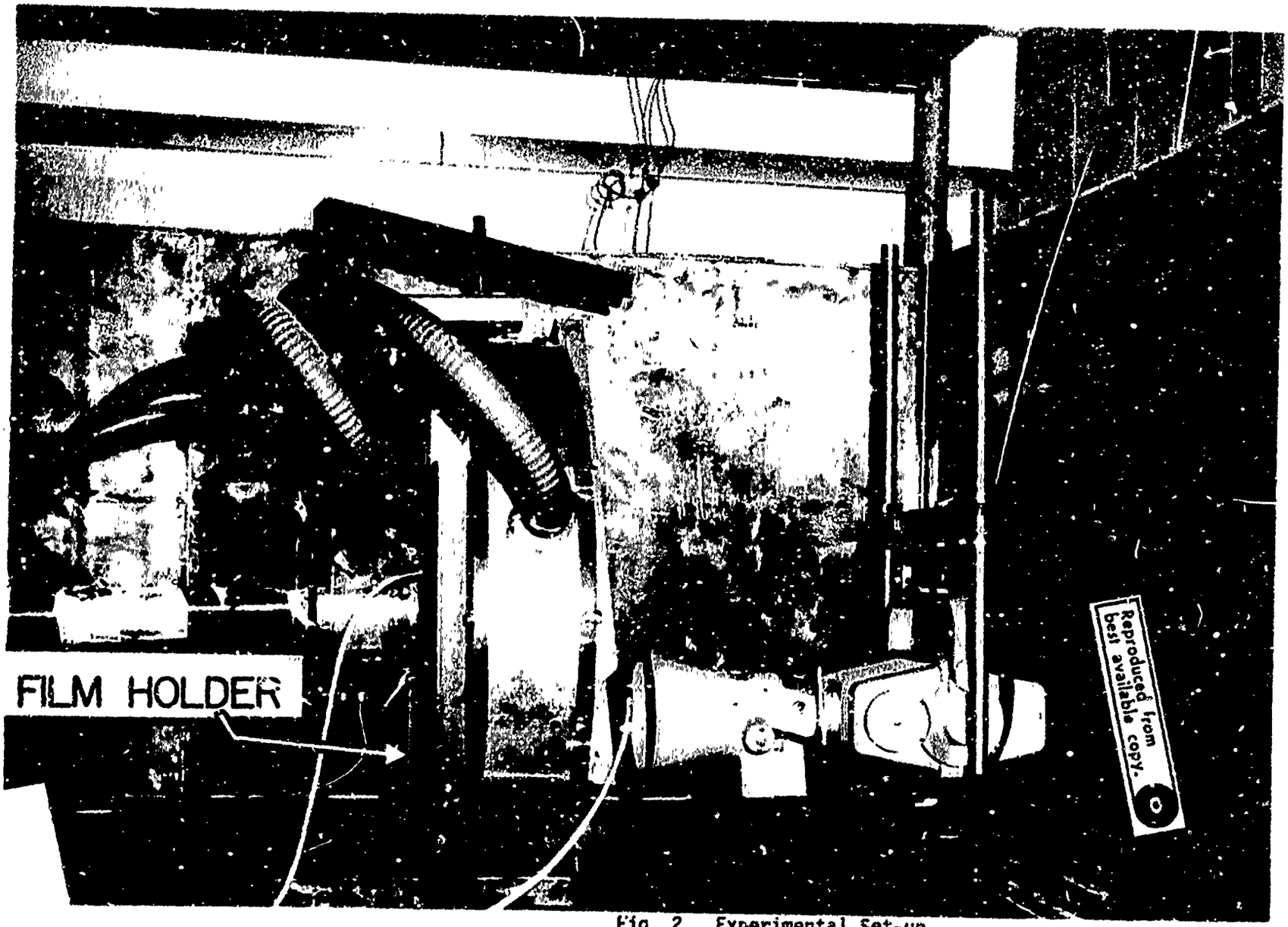

Fig. 2 Experimental Set-up

up to 50 inches, this lead box had dimensions of approximately 73" x 49" x 38". These dimensions limited the source-to-object distance to some 20 inches. The box was built from plywood covered with 1/16" thick lead sheet. A double thickness of lead on the side exposed to the direct X-ray beam insured that the direct beam was adequately attenuated. Two small access doors were used for service adjustments and film changes during an experiment. The complete X-ray system, set up for observation of powder flow in a vortex chamber, is shown in Figure 2.

The photographic film density was measured by the photodensitometer shown schematically in Figure 3. Photographic density is defined as the $\log_{10}$ of the ratio of intensity of incident light to transmitted light through the radiograph (exposed film). These intensities were detected by a photomultiplier tube, and indicated on the Y-axis of an X-Y recorder. A Spectra Physics 131 He-Ne gas laser was used as the light source. By using a laser source, a 2 mm spatial resolution was obtained without the tedious alignment and focusing associated with lens-aperture devices. However, there is a danger in producing consistently erroneous results with the laser-photomultiplier system. This problem arises from the high power density associated with the laser beam, and the possibility of overloading, or choking, the pnotomultiplier system. The effect of photomultiplier choking is illustrated in Figure 4. A test film was scanned under normal, non-choked, operating conditions (photomultiplier voltage at 565 v) with the transmitted intensity given by curve 1. When the photomultiplier voltage was increased

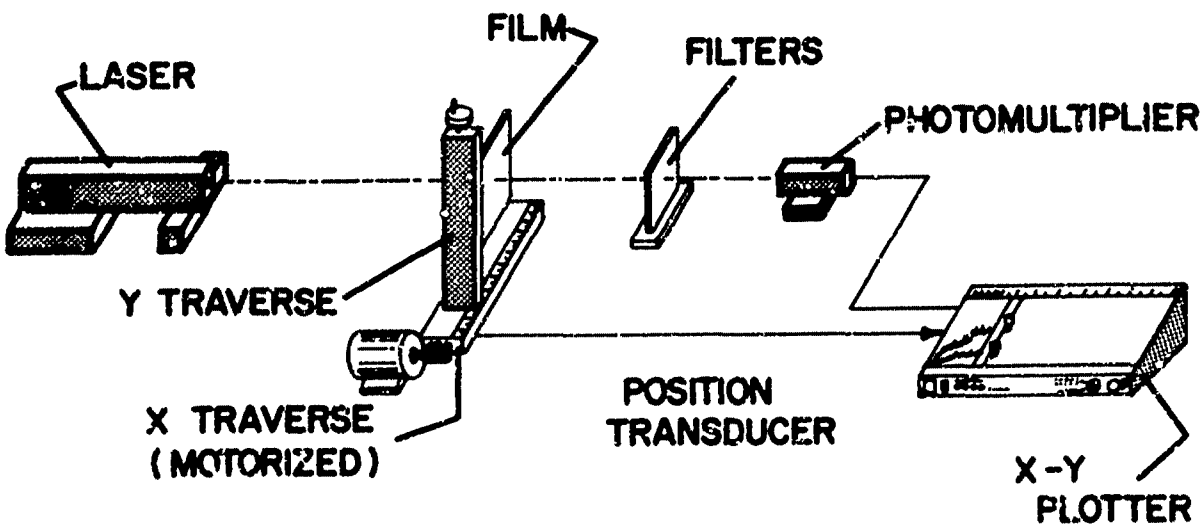

Fig.3 PHOTODENSITOMETER SCHEMATIC

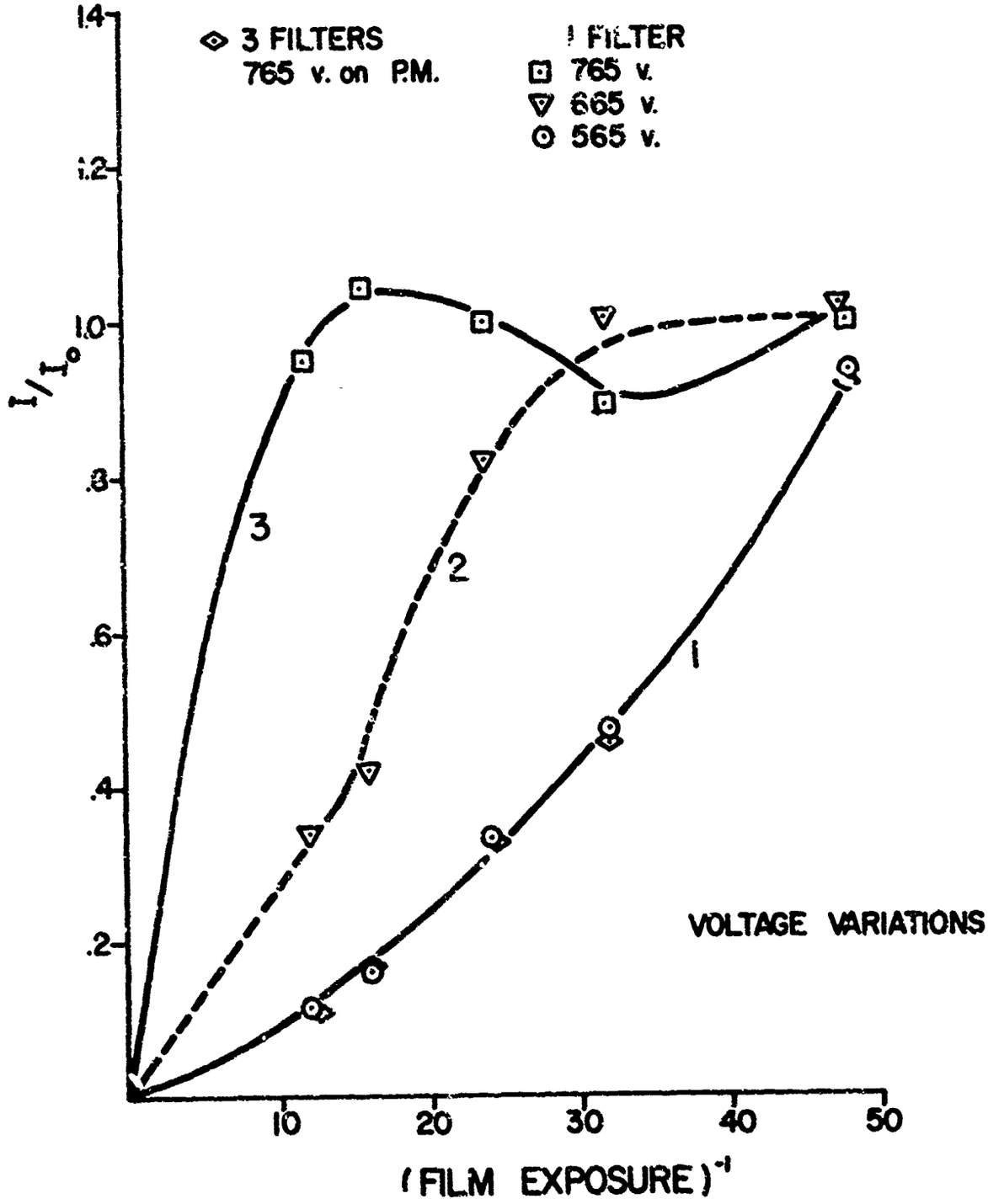

Fig. 4 Photodensitometer Readings under "choked" conditions

to some 660 v, the apparent intensity followed curve 2: the photomultiplier choked, indicated a decreasing intensity over a certain range, and then gradually recovered. This erroneous curve was accurately repeatable: therefore much care must be taken to insure that one does not unknowingly extend the photomultiplier into this choke range. Much time was spent with the photodensitometer, varying photomultiplier voltage and laser beam intensity (by varying beam filter thickness) to insure tnat the system did not choke under normal operation.

The film was mounted on a two-dimensional traverse, with manual adjustment in the vertical direction, and motor-driven movement in the horizontal direction. A position transducer connected to the X-axis of the X-Y recorder provided direct plotting of light beam intensity as a function of horizontal position. With this arrangement, a series of horizontal scans at various heights could be taken to obtain two-dimensional plots of film density.

III. EXPERIMENTAL ANALYSIS

The Absorption Process

When an X-ray beam of intensity I passes through a thickness of material $d\ell$, the beam intensity is decreased by an amount

$$\frac{dI}{I} = -\mu_\ell d\ell \tag{1}$$

where μ_ℓ is the linear absorption coefficient for the material. Therefore, the intensity of a beam which has passed through a length of material, ℓ, is

$$I = I_o \exp(-\mu_\ell \ell), \tag{2}$$

I_o is the initial intensity of the beam. In X-ray absorption work, it is customary to use the mass absorption coefficient, μ_m, which is the linear absorption coefficient divided by material mass density. Equation 2 can then be rewritten:

$$\mu_m \rho = \frac{-1}{\ell} \ln(I/I_o) \tag{3}$$

When μ_m for a given material is known, this equation can be used to relate X-ray beam attenuation to mass density of material. The mass absorption coefficient for a given material is determined from atomic mass absorption coefficients, which can be obtained from X-ray physics tables (see Appendix). Equation 3 is the basis for our measurements of particle density in multi-component flow.

Many secondary effects can complicate this relatively simple process. For instance, mass absorption coefficient is dependent on wavelength, and "white" radiation (bremsstraghlung) is employed in our X-ray experiment (that is, no attempt was made to limit wavelength range of radiation). This problem is discussed in detail in the Appendix. Use of a broad, diverging beam can also introduce errors in an absorption measurement (Reference 9). Additional errors may arise from small-angle scattering (Reference 10), particularly when nonhomogeneous medium is studied (Reference 11). In view of these complications, calibration tests were made to determine the mass absorption coefficient for talc powder (the powder used in flow experiments described in the next section), and possible variations of this coefficient over the range of particle density and beam attenuation covered in flow tests. Incident intensity and transmitted intensity of a beam passing through a talc bed thickness of 3.0 cm was measured. From these measurements, the mass absorption coefficient for talc was calculated as 0.71 cm^2/gm (details of this analysis are given in the Appendix). This calibration can be performed for other powders that may be of interest in flow tests: the Appendix lists approximate μ_m values from X-ray tables for a number of materials.

Intensity Data from Photographic Film

The photographic recording technique has several advantages and disadvantages when used for quantitative analysis. On the positive side, intensity data over a wide test area can be collected quickly and efficiently with film; time-averaged data is obtained from film, thus

smoothing out statistical fluctuations in the process measured; equipment investment is nominal; and the film data format can be directly used for qualitative visualization of flow patterns. There is also the debit side: at large film density, the recorded density is no longer linearly related to X-ray exposure; sensitivity may vary from one film to the next; development procedures must be consistent for all films; and film granularity may produce an inherent noise level in the system. Before the photographic process can be used for accurate intensity measurements, these problem areas must be analyzed to define proper ranges of application and practical operating limits.

As mentioned earlier, Kodak type AA X-ray film was used for our experiments. Our standard developing procedure was: 5 min developer, 40 sec stop bath, 5 min fixer, and 30 min wash. Developer temperature was at room level, 68°F ± 2°. According to Kodak film data (Reference 12), this variation in temperature could give as much as 3% change in film speed.* In normal operation, we developed some 20 films (5" x 7" area) with one gallon of X-ray developer, with no noticeable decrease in chemical strength.

When the photographic process is used for quantitative analysis, the relationship between X-ray exposure and resultant film density becomes quite important. The term "exposure" as used here means the product of radiation intensity and time of the exposure. A common problem in optical

*If development time is varied to compensate for temperature changes (as suggested in Reference 12), this film speed error can be further reduced.

photography is the failure of the reciprocity law at low intensity levels (Reference 13), which may lead to nonlinearity in the density-exposure curve at low exposures. This effect does not occur in X-ray work, because of the large energy associated with the X-ray photon. Therefore the density-exposure curve for X-rays is expected to be linear for small exposure. An experimental determination of film density as a function of X-ray exposure (constant intensity and variable exposure time) is shown in Figure 5. This curve is linear up to a film density of about 1.5, with the slope of the curve decreasing rapidly as density increases above 1.5. The shape of the curve agrees well with film characteristics reported in Reference 14. This curve could be used to calibrate measured density to relative exposure over the full range of density from 0 to 2.5 or so. Whenever possible, it is better practice to limit film density to the linear region of the curve.

Error Analysis

Calculation of flow density from this X-ray data must follow four principal steps: (1) measurement of light transmission through photographic film, (2) conversion of light transmission data to photographic density, (3) comparison of exposure, E, of the attenuated and unattenuated beams, (4) and finally application of the mass absorption coefficient to obtain flow density values. Each of these steps can introduce error into the experiment, and each step will be analyzed in this section.

The photographic density of a film is defined as

$$D \equiv -\log_{10} J/J_0 \qquad (4)$$

where J_0 is incident light beam intensity and J is intensity of beam after passing through the film. As described in the preceeding section, J and J_0 were measured with a laser-photomultiplier system. Reproducibility of intensity data was studied by making 10 scans of an X-ray picture of a column of plastic balls (about 1/8" diameter balls). The photograph of the packed bed of plastic balls made a good test subject for intensity readings, because of large intensity gradients produced by voids between spheres. Two of the ten intensity scans are shown in Figure 6: these curves were chosen to show the maximum deviation observed in the test. Intensity readings were taken at 20 points along the scan: standard deviation, σ_J, was found to be 1% of the intensity reading J. Part of this error appeared to be a slight scale shift from one run to the next. We anticipate that minor improvements in electronic equipment, such as a regulated power supply, could improve the reproducibility of intensity measurements considerably.

Variations in radiographic density values recorded on successive films were checked by making ten exposures of a calibration subject. The calibration subject was a series of strips of electrical tape, with varying thicknesses to give steps of increasing density on the exposed film. Average standard deviation, σ_D, over 45 reference points on the pattern, was 2% of the recorded density. A series of radiographs of the flow chamber, with no air or powder flow, was also made to test film density variation: again the result was 2% of the recorded density. This error is somewhat above that expected from intensity error propagation, so that

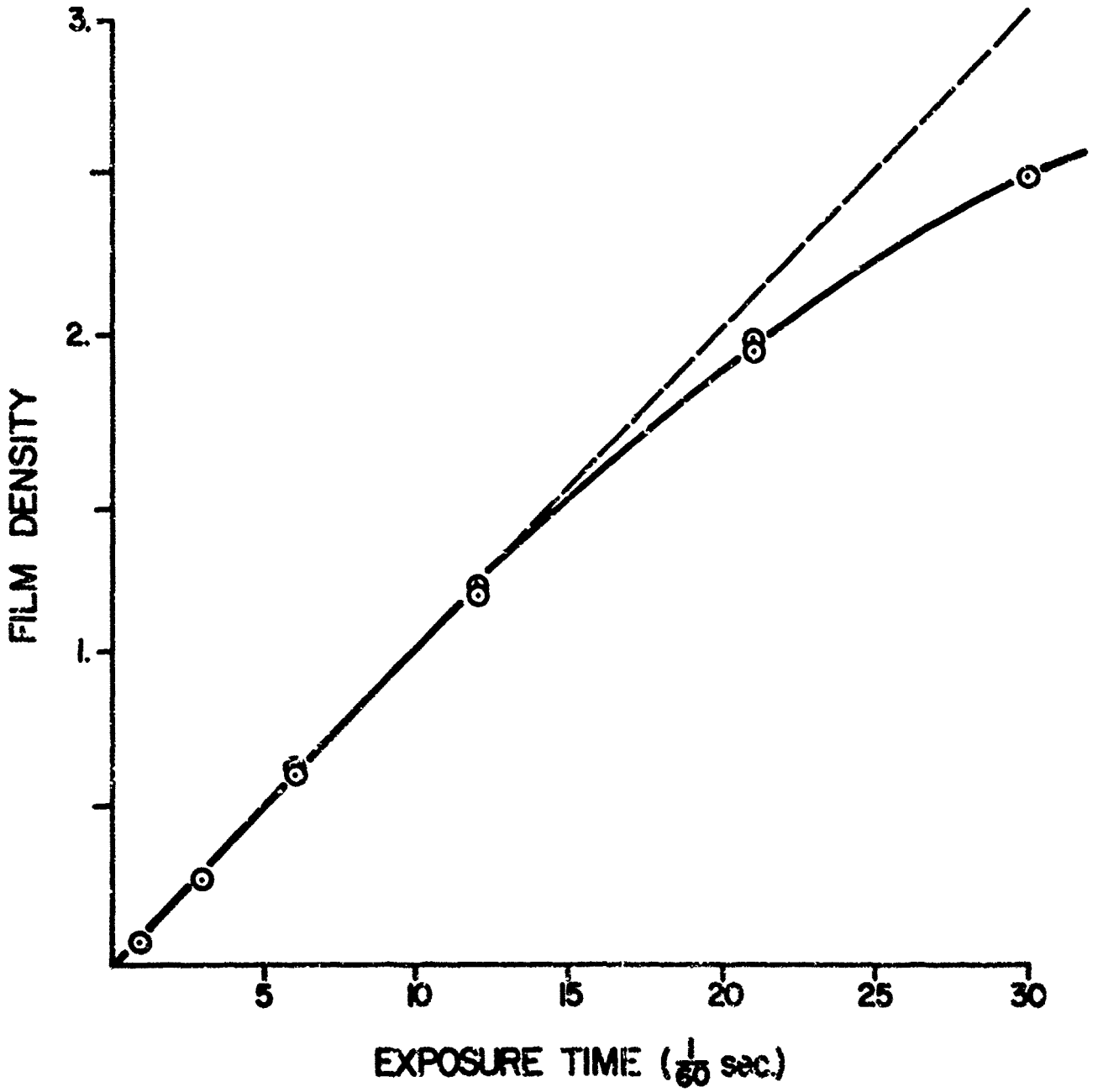

Fig. 5 Film Density versus Exposure Time

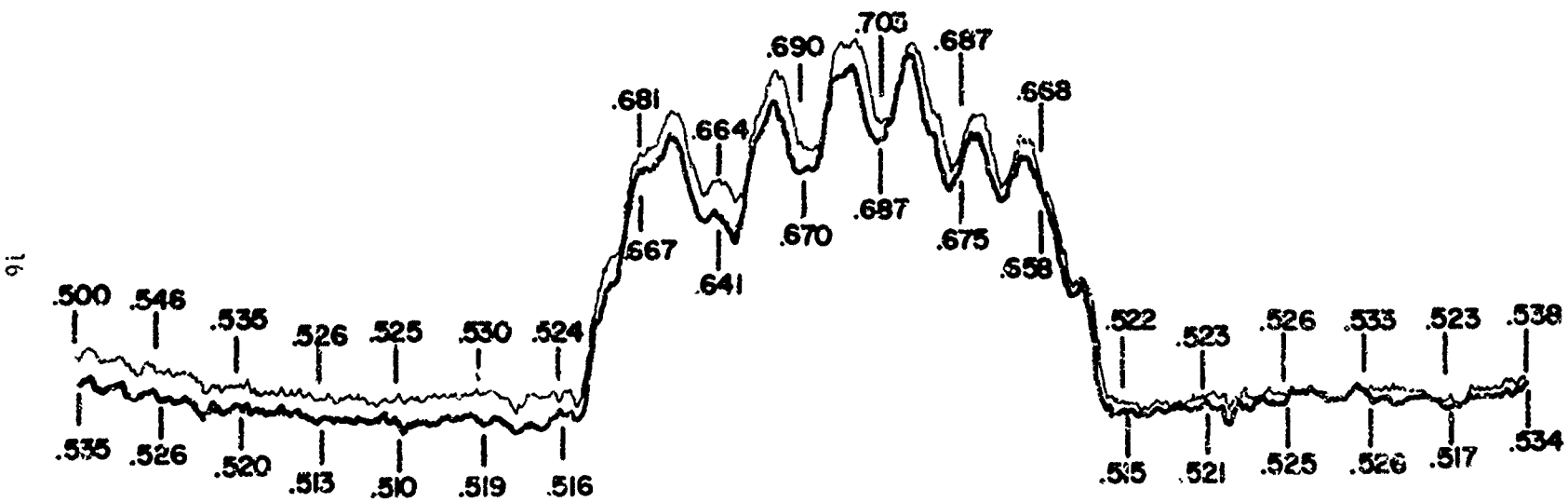

Fig. 6 Signal Variation from Photodensitometer

film sensitivity and film processing appear to contribute some 1% error in this experiment.

The final step in the calculation is the determination of flow density, ρ, from Equation 3. The beam intensity, I, shown in Equation 3 must be obtained from film density data. As shown in Figure 5, intensity is linearly related to film density, D, for $D \leq 1.5$. When film density is below that value,[+] then, Equation 3 can be expressed as

$$\rho\ell = -\frac{1}{\mu_m} \ln D/D_0 \qquad (5)$$

Propagation of error in measuring D should give about 4% variation in the determination of $\rho\ell$. The standard deviation in a series of powder flow experiments was found to be about 4% of the mean value. The absolute value of $\rho\ell$ is determined when absorption coefficient μ_m is known. As described in the Appendix, calibration tests were made to obtain μ_m for the powder used in the flow experiment. Standard deviation of those calibration tests was also 4%. Table 1 presents a summary of these experimental errors.

+If D is extended above the linear range, substantial error may arise from D-E calibration error as well as increased sensitivity of the calculation to error in D. For that reason, we will limit our discussion to the linear region of the D-E curve.

Table 1

Standard Deviations of Experimental Measurements

Light Intensity	σ_J/J = 01
Radiographic Density Determination	σ_D/D = 0.02
Flow Density Calculation	σ_ρ/ρ = 0.04

The maximum and minimum powder densities that can be measured by this process are determined by error limits. The minimum measurable powder density is reached when attenuated X-ray intensity is lower than the unattenuated intensity by the amount σ_D: that is,

$$(\rho\ell)_{min} = \frac{-1}{\mu_m} \ln \frac{D_o - \sigma_D}{D_o} \tag{6}$$

Since $\sigma_D/D \ll 1$, this is approximately

$$(\rho\ell)_{min} = \frac{1}{\mu_m} \frac{\sigma_D}{D_o} \tag{7}$$

With 2% standard deviation, and powder absorption coefficient of 0.7 cm^2/gm, the minimum observable value of $\rho\ell$ is about 0.03 gm/cm^2. The maximum measurable powder density is somewhat more ambiguous than the previous example. A large film density span is required: because of nonlinearity of the D-E curve (Figure 5), the highest film density must be limited to something like 2. The smallest film density that can be accurately read is determined by measurement error in light beam intensity.

$$D_{min} = \log \frac{J_o - \sigma_j}{J_o} \quad ,$$

$$\text{or} \quad D_{min} = 0.43 \frac{\sigma_j}{J_o} \quad . \qquad (8)$$

This figure is $D_{min} \sim 0.005$, giving maximum powder density of

$$(\rho\ell)_{max} = \frac{-1}{\mu_m} \ln \frac{0.005}{2}$$

and again using $\mu_m = 0.7$ cm^2/gm, $(\rho\ell)_{max} \approx 9.$ gm/cm^2.

An estimate of spatial resolution obtainable with the Kodak AA film was made from X-ray shadowgraphs of tungsten powder. Particle sizes of the tungsten ranged from 1 micron to more than 100 micron, and the particles had angular, irregular shape. An enlargement of the shadowgraph showed very good reproduction of the jagged shapes of 100 micron tungsten particles, but particles as small as 10 microns were at the limit of distinct resolution.

IV. DENSITY MEASUREMENTS OF POWDER IN VORTEX FLOWS

As examples of the application of the X-ray absorption technique to aerodynamic tests, density measurements of powder-laden vortex flows will be presented. The vortex chamber is shown in Figure 2: outer radius of the chamber was 15 cm, and the chamber was modified for axial lengths of 6.3 cm, 12.6 cm, and 18.9 cm. As described in Refs. 15 and 16, the purpose of measuring powder densities in vortex flows was to determine both uniformity and magnitude of the density within the flow.

Positive prints of radiographs of a portion of the vortex flow near the outer radius are shown in Figures 7 and 8. Solid black sections of the photograph are vanes which make up the outer cylindrical wall of the chamber, and also provide tangential slots for gas injection to drive the vortex (see Figure 9). The first photograph shows the flow established with 200 gm of talc powder in the chamber: the second photograph is with 600 gm powder in the chamber. The average powder density appears to remain fairly constant, with the powder zone thickness increasing with increased powder load. A striking feature of these photos is the rather low density of powder at the vane. This low density region is probably generated by the particle-free gas injection at the vane. Because of the large wall torque produced by powder flow in contact with container surfaces, the existence of this low density region leads to significantly larger angular velocity than had been anticipated.

Numerical calculations of powder density were possible when the unattenuated beam intensity was determined. Figure 9 shows an X-ray

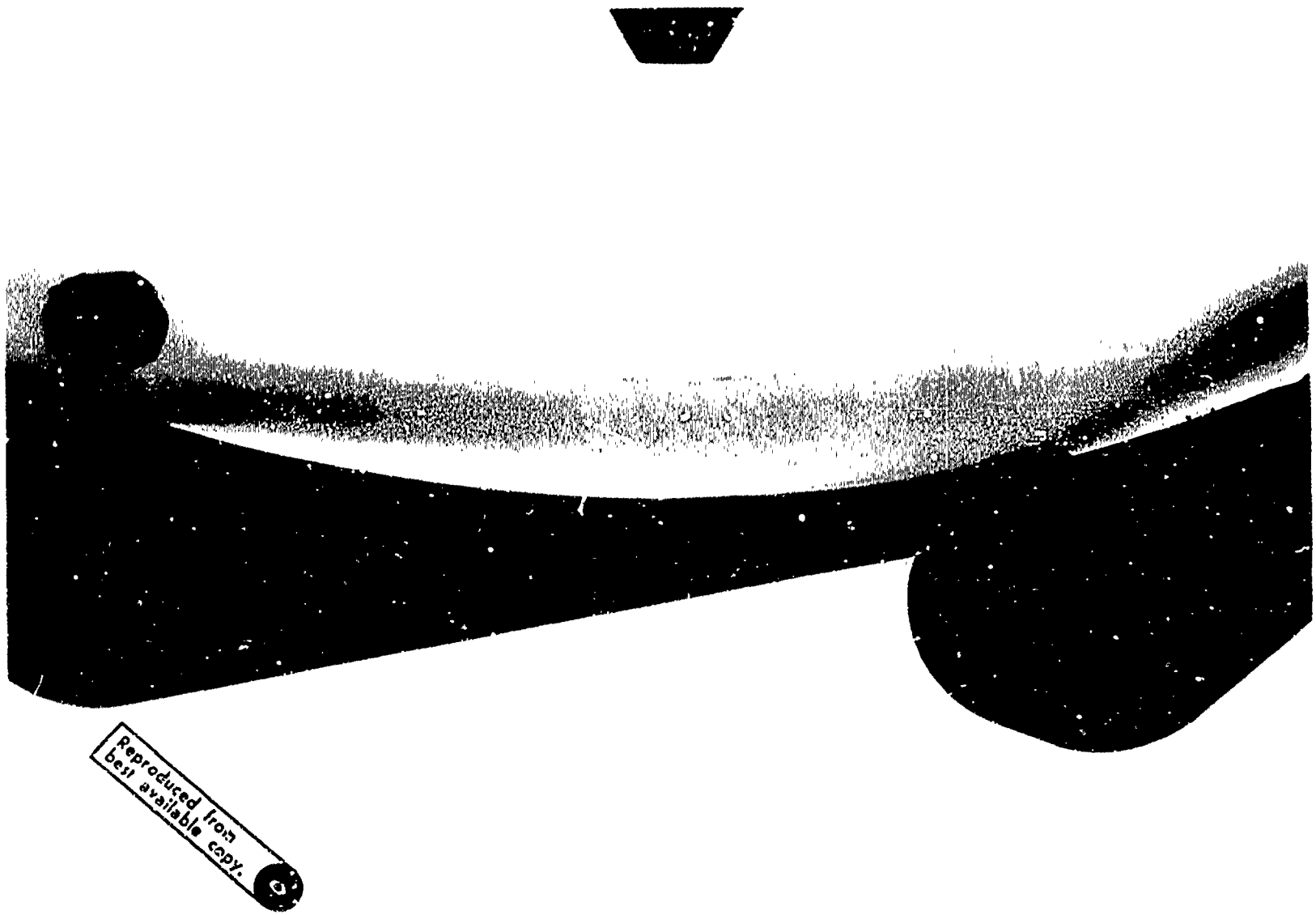

Fig. 7 Radiograph of Vortex
Flow: 200 gm powder

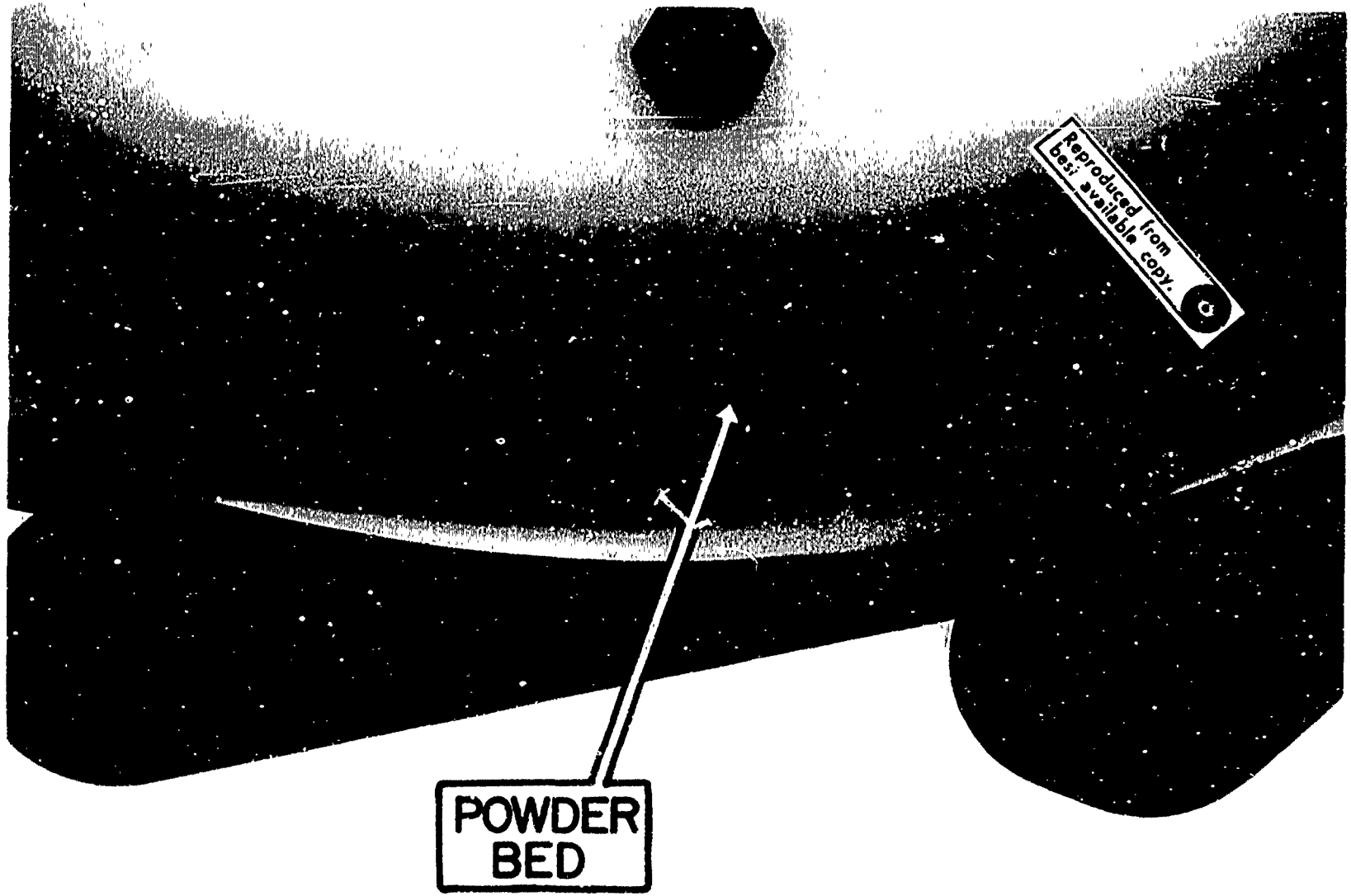

Fig. 8 Radiograph of Vortex
Flow: 600 gm powder

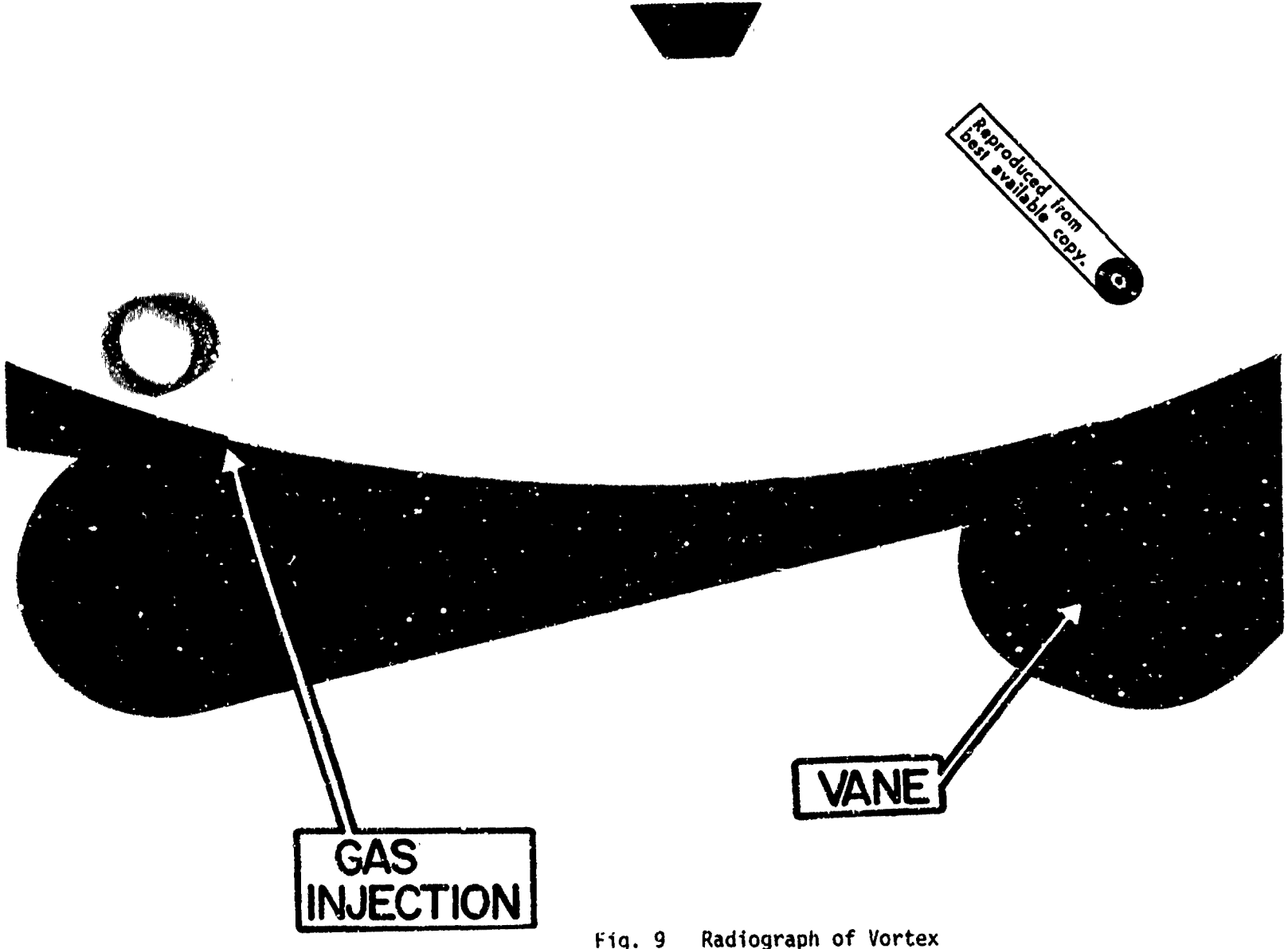

Fig. 9 Radiograph of Vortex Chamber: No powder

photograph of the vortex chamber with no flow. Radiographic density measurement of this no-flow condition gave the required D_o needed in Equation 5, and corresponding photographic density measurement of the flow photograph gave D. Equation 5 was then used to calculate powder density ρ. Figures 10-14 show a series of powder density contours calculated by this method. Total powder load for these cases was 400 gm, with a variety of gas injection flow rates. These contours show how the large density islands above the injection slots are reduced as gas flow rate through the slots, $\dot{m}_{CR}$, is increased relative to the flow rate of gas injected through nozzles at a radius of 2 inches, $\dot{m}_{ew}$. (For details, the reader should consult Reference 15. The intent of this presentation is not to describe the vortex flow, but to show the utility of the X-ray absorption analysis).

Powder density profiles along the chamber radius, halfway between the gas injection slots, are shown in Figure 15 for a number of different total powder loads. In Figure 16, data from three different axial chamber lengths are presented. The profiles were expected to be similar for constant $\dot{M}/\ell$, and this did prove to be the case. The axial chamber length, ℓ, is also the absorption path length, so this similarity in profiles indicates that the analysis is little affected by absorption length variation.

The X-ray process may have important uses for visualizing flow processes that must be contained within metal containers, for reasons of high pressure or electrical or radiation isolation. The X-ray beam could

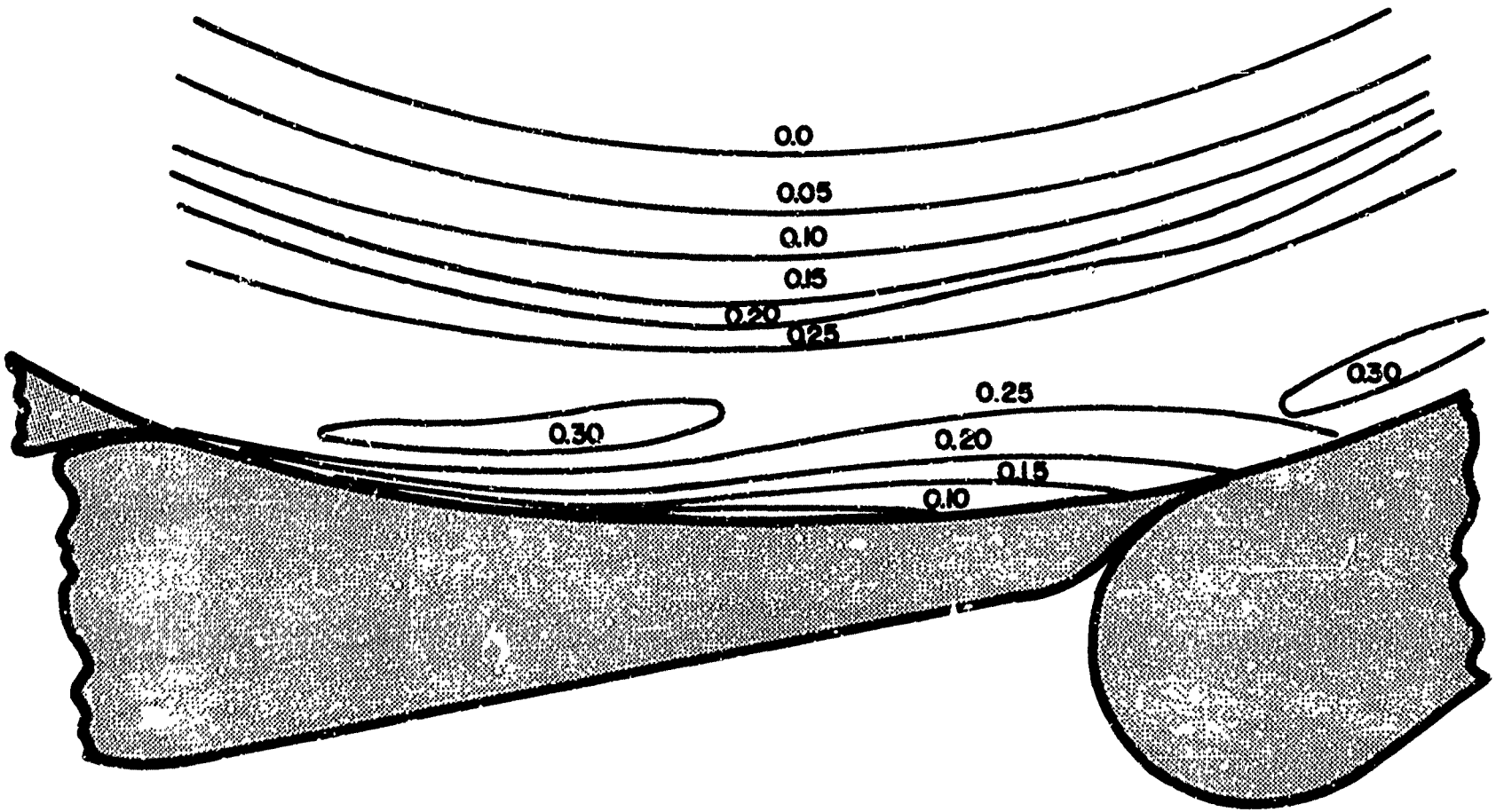

Fig. 10 Density Contours: $\dot{m}$ = 160 gm/sec, $\dot{m}_{ew}/\dot{m}$ = 0.33

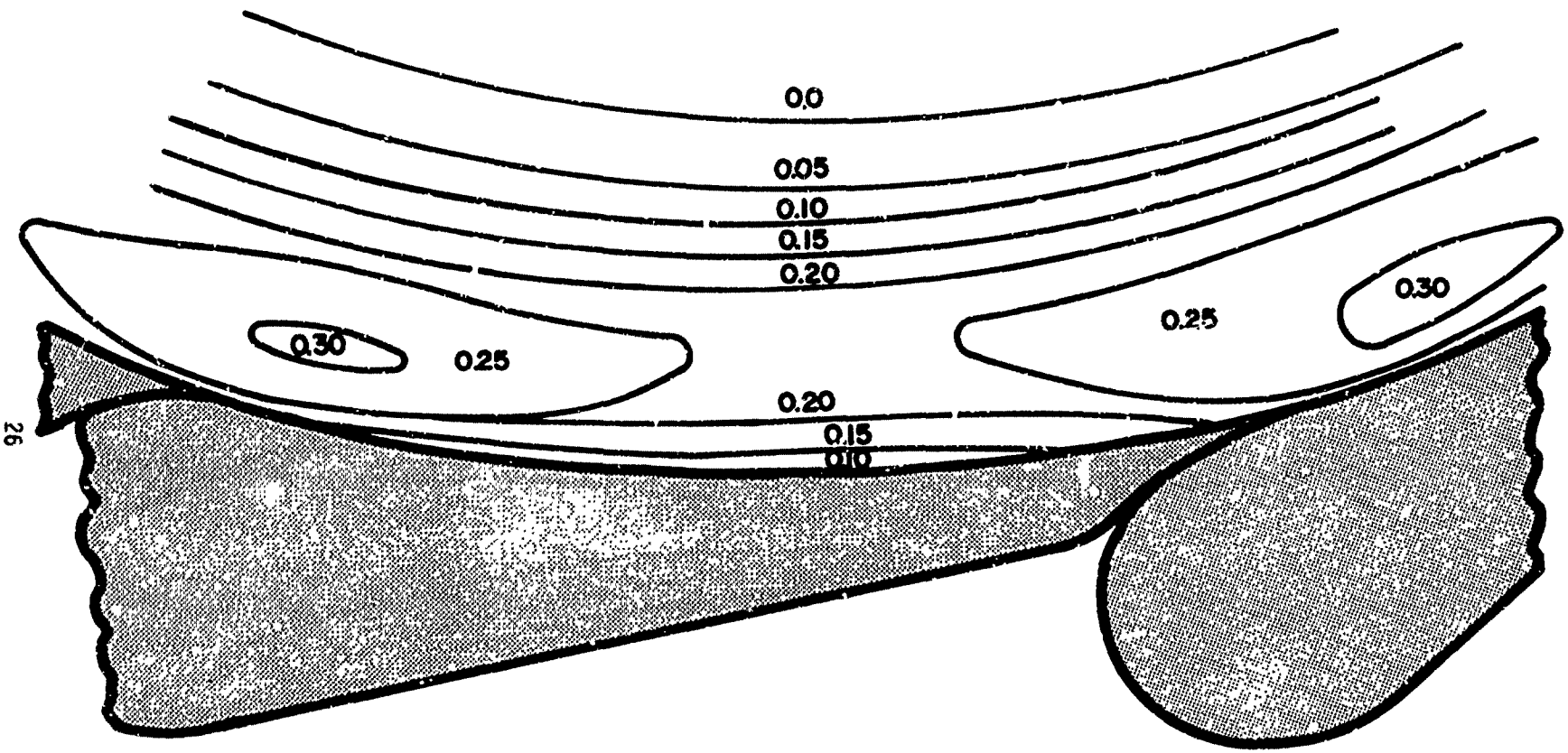

Fig. 11 Density Contours: $\dot{m}$ = 160 gm/sec, $\dot{m}_{ew}/\dot{m}$ = 0.67

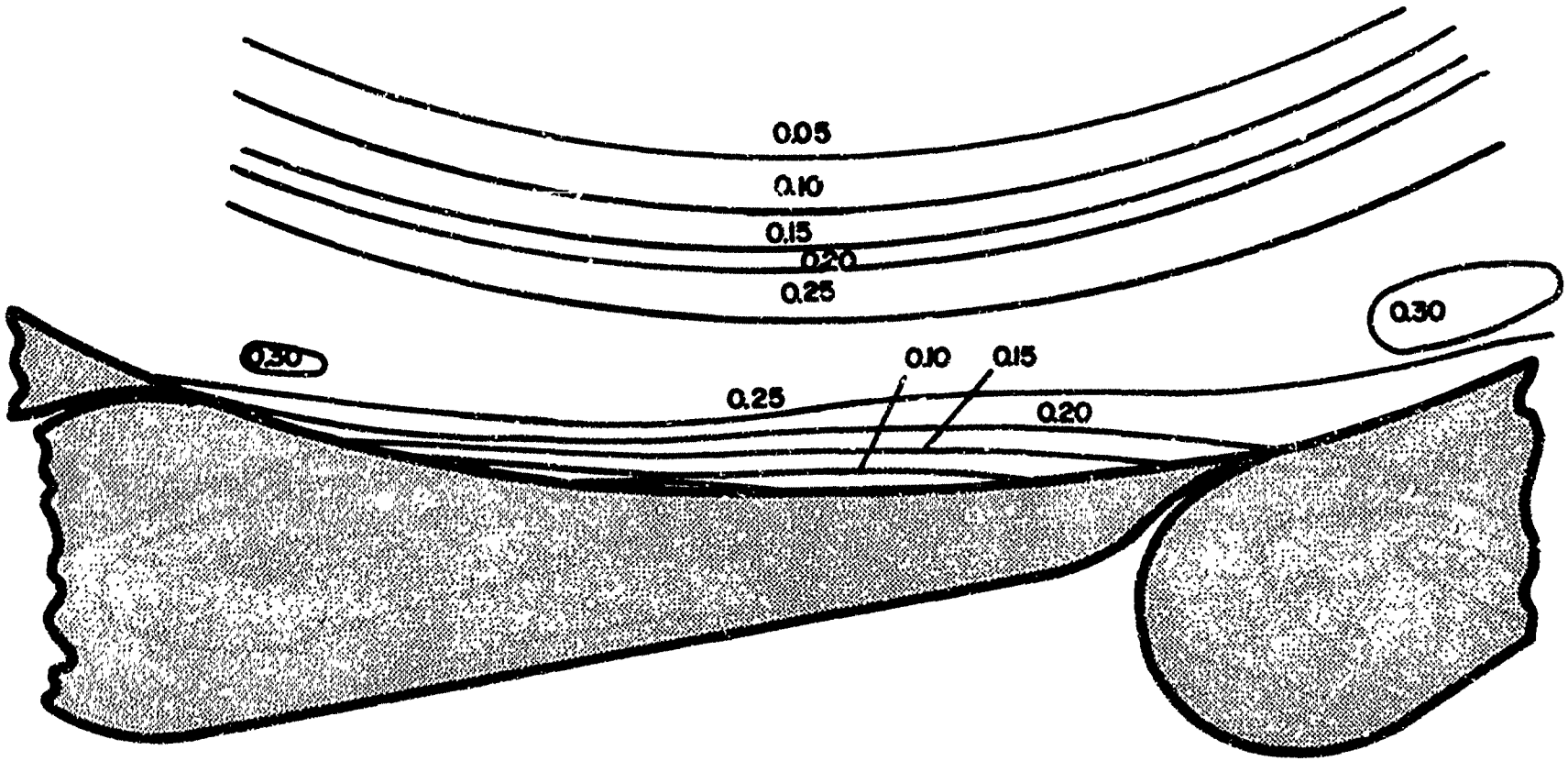

Fig. 12 Density Contours: $\dot{m}$ = 135 gm/sec, $\dot{m}_{ew}/\dot{m}$ = 0.4

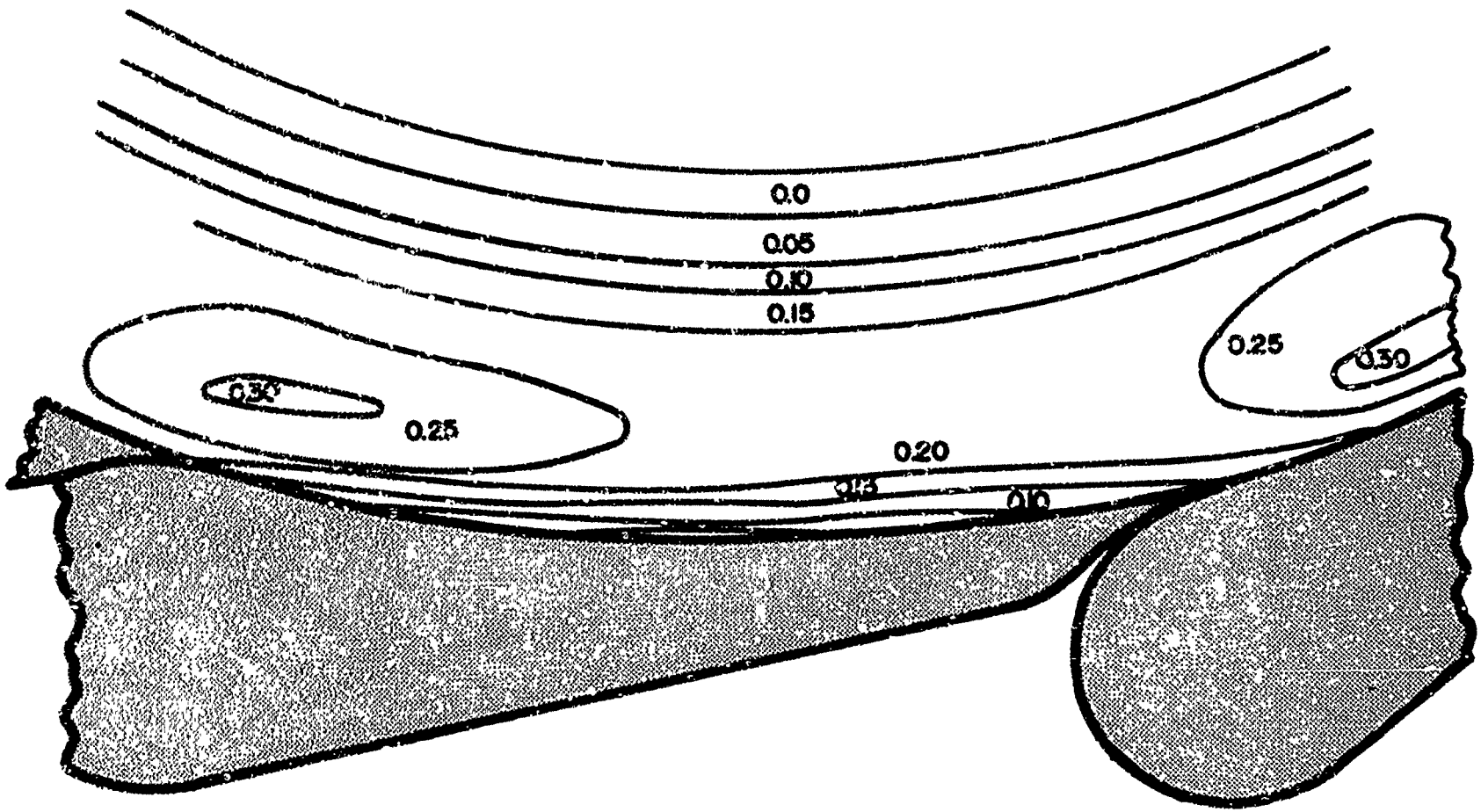

Fig. 13 Density Contours: $\dot{m}$ = 135 gm/sec, $\dot{m}_{ew}/\dot{m}$ = 0.5

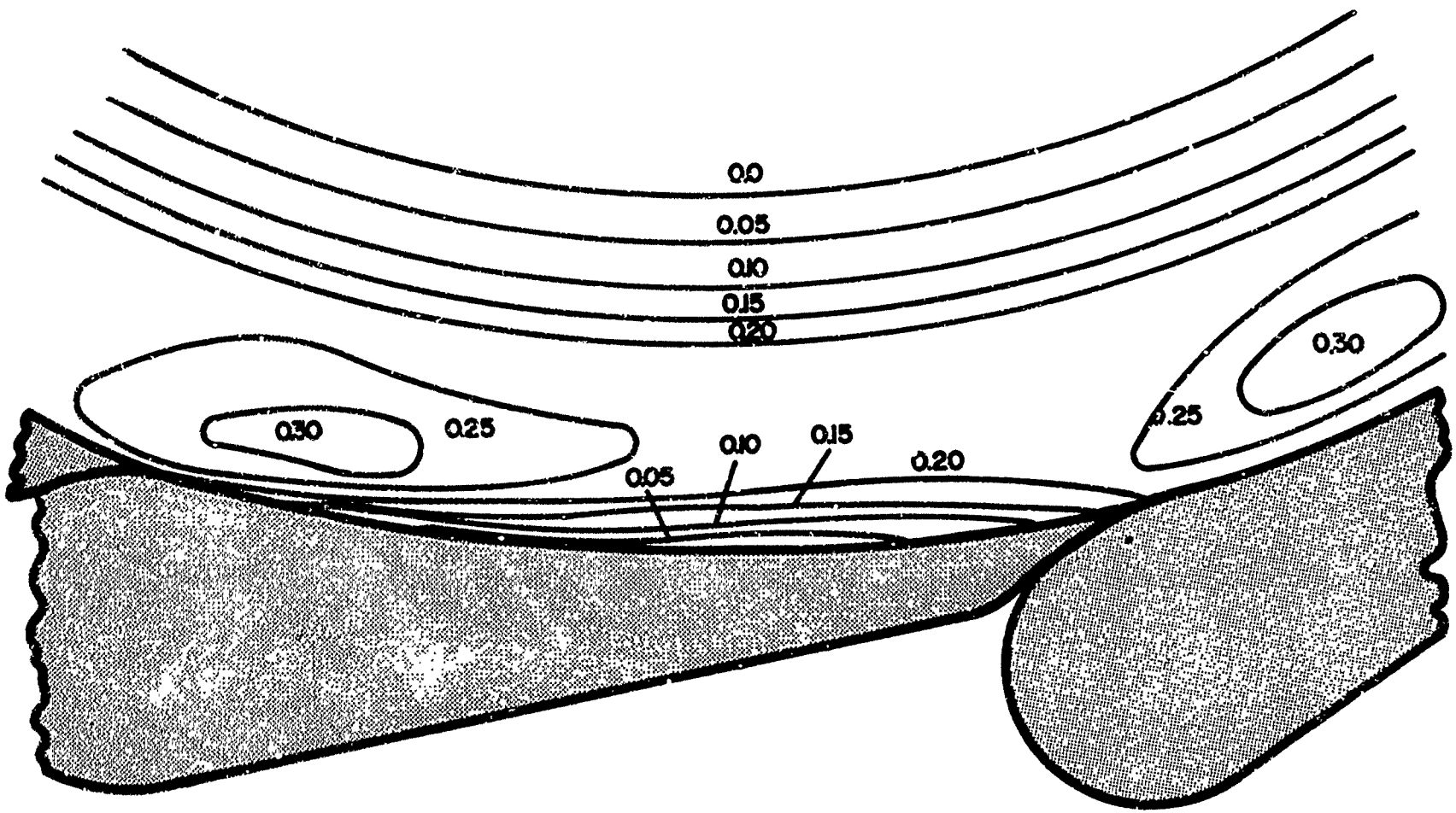

Fig. 14 Density Contours: $\dot{m}$ = 135 gm/sec, $\dot{m}_{ew}/\dot{m}$ = 0.6

be transmitted through aluminum or brass walls, with sufficient intensity to record density variations within the internal flow.

The theoretical analysis presented here has shown that the X-ray absorption process is capable of producing reliable, accurate density data for multi-component flow experiments. The experimental data shown here has verified that analysis. Qualitative photographs, such as Figures 7 and 8, have had considerable impact on our understanding and formulation of the multi-component vortex flow. Quantitative data, such as Figures 15 and 16, have helped to test the accuracy of such formulations. Measurement errors encountered in these experiments could be substantially reduced by more refined procedures. The medical X-ray source used here was not particularly designed for extreme accuracy, our photographic processing techniques can be improved considerably, and more X-ray beam filtration could further reduce the absorption coefficient uncertainties.

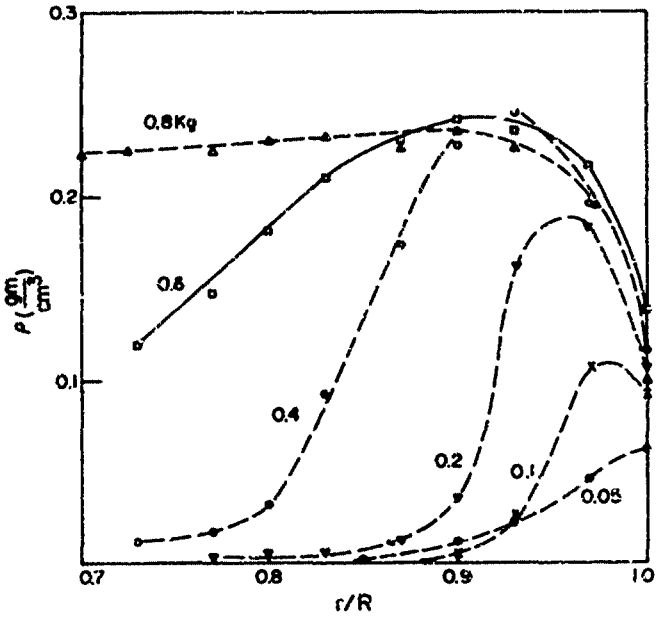

Fig. 15 Radial Profile of Density
$\dot{m}$ = 135 gm/sec

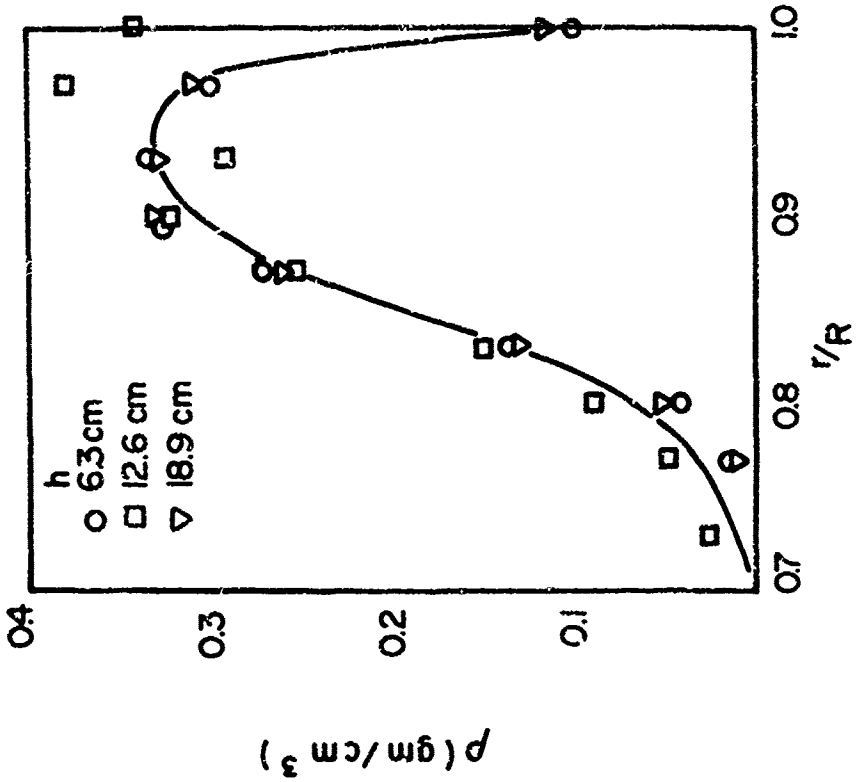

Fig. 16 Radial Profile of Density: $\dot{m}$ = 160 gm/sec

V. REFERENCES

1. Winkler, Eva M., "Density Measurements in Supersonic Flow by Means of the X-ray Absorption Method", Journal of Applied Physics, 22, 201 (1951).

2. Kistiakowsky, G. B., and P. H. Kydd, "Gaseous Detonations IX. A Study of the Reaction Zone by Gas Density Measurements", Journal of Chemical Physics, 25, 824 (1956).

3. Dapoigny, J., J. Kieffer, and B. Vodar, "Some Results Relating to the Compression of Water in a Shock Wave", C.R. Acad. Sci., 238, 215 (1954).

4. Rowe, P. N., and B. A. Partridge, "An X-ray Study of Bubbles in Fluidized Beds", Transactions of the Institution of Chemical Engineers, 43, 157 (1965).

5. Rowe, P. N. et al, "The Mechanisms of Solids Mixing in Fluidized Beds", Transactions of the Institution of Chemical Engineers, 43, 271 (1965).

6. Botterill, J. S. M., J. S. George, and H. Besford, "Bubble Chains in Gas Fluidized Beds", Fluid Particle Technology (Chemical Engineering Progress Symposium Series), 62, 7 (1966).

7. Matsen, J. M., S. Hovmand, and J. F. Davidson, "Expansion of Fluidized Beds in Slug Flow", Chemical Engineering Science, 24, 1743 (1969).

8. Oliver, J. P., G. K. Hickin, and Clyde Orr, Jr., "Rapid, Automatic Particle Size Analysis in the Subsieve Range", Powder Technology, 4, 257 (1970).

9. Compton, Arthur H., and Samuel K. Allison, "X-Rays in Theory and Experiments", Second Edition, D. Van Nostrand Company, Inc., New York (1935).

10. Chipman, D. R., "Mass Absorption Coefficient of Carbon for Cu Kα Radiation", Journal of Applied Physics, 26, 1387 (1955).

11. Parratt, L. G., J. O. Porteous, H. W. Schnopper, and T. Watanabe, "X-ray Absorption Coefficients and Geometrical Collimation of the Beam", Review of Scientific Instruments, 30, 344 (1959).

12. "Kodak Products for Industrial Radiography", Eastman Kodak Company, Rochester, New York.

13. Mees, C. E. Kenneth, "The Theory of the Photographic Process", MacMillan Co., New York, (1954).

14. "A Comparison of Various Commercially Available X-ray Films", Acta Crystallographica, 9, 520, (1956).

15. Anderson, L. A., S. Hasinger, and B. N. Turman, "Two Component Vortex Flow Studies, with Implications for the Colloid Core Nuclear Rocket Concept", AIAA Paper No. 71-637, AIAA/SAE 7th Propulsion Joint Specialist Conference, Salt Lake City, Utah, June, 1971.

16. Turman, B. N., and S. H. Hasinger, "Experimental Flow Studies of the Colloid Core Reactor Concept", Proceedings, 2nd Symposium on Uranium Plasmas, Atlanta, Georgia, November 1971.

17. "Nuclear Data", Vol. 7, No. 6, U.S. National Bureau of Standards, 1970.

VI. APPENDIX

The mass absorption coefficient, μ_m, for the elements is given in any number of X-ray physics texts and handbooks, for example, References 9, 17. As explained in Reference 9, mass absorption coefficients for a compound, μ_c, is calculated from absorption coefficients for the component element, μ_x, and relative mass concentration of the element, C_x:

$$\mu_c = \Sigma_x \mu_x C_x \quad . \qquad \text{A1}$$

The mass absorption coefficient for a given material is dependent on the wavelength, λ, of incident radiation. An example of this dependence is shown in Figure A1, which shows μ_m for magnesium, one of the principal ingredients of talc.† The continuum, or bremsstrahlung, radiation from an X-ray tube covers a wide range of wavelengths, with an intensity distribution similar to the I_o curve sketched in Figure A2. Since the continuum radiation has no one well-defined wavelength, the resultant absorption coefficient is an average over the total spectrum. An important consequence of this average is the fact that the mean absorption coefficient, $\bar{\mu}_m$, is dependent on the total fraction of the X-ray beam that is absorbed.

The proper averaging for μ_m can be derived from Equation 1, expressed in terms of discrete wavelengths:

$$dI^\lambda = -\rho\mu^\lambda I^\lambda d\ell \quad . \qquad \text{A2}$$

†Chemical composition of talc is $3MgO.4SiO_2.H_2O$. Principal absorbers are Mg and Si: μ_m for Si is near that of Mg.

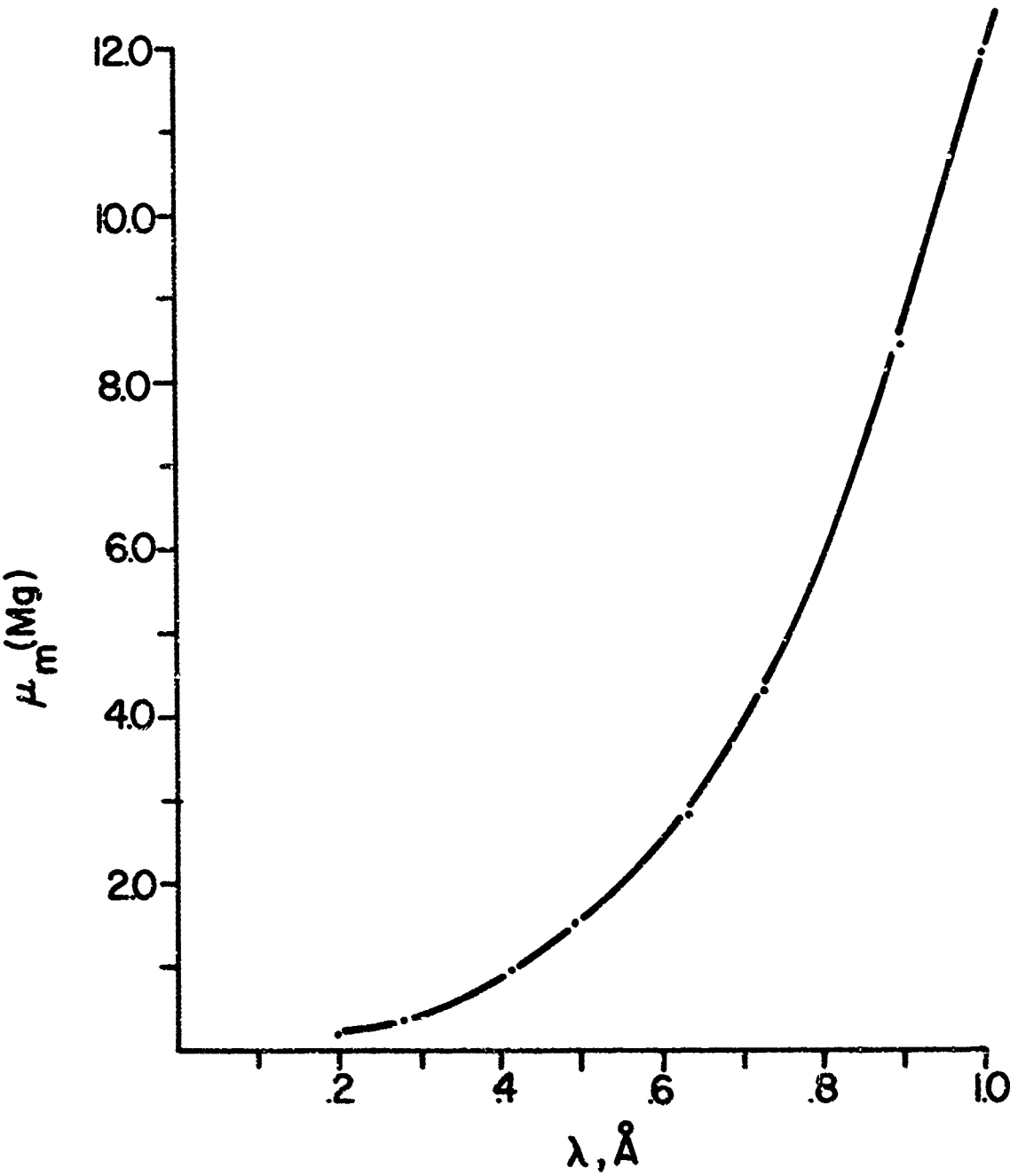

Fig. A1 Mass Absorption Coefficient for Mg as a Function of Wavelength

The total absorption experienced over length $d\ell$ is

$$\Sigma dI^{\lambda} = -\rho d\ell \Sigma \mu^{\lambda} I^{\lambda} \quad . \qquad \text{A3}$$

Dividing both sides by ΣI^{λ}, we have

$$\frac{\Sigma dI^{\lambda}}{\Sigma I} = -\rho \frac{\Sigma \mu^{\lambda} I^{\lambda}}{\Sigma I} d\ell \quad , \qquad \text{A4}$$

which takes the form of Equation 1 when the mean absorption coefficient is defined by

$$\bar{\mu}_m = \frac{\Sigma \mu^{\lambda} I^{\lambda}}{\Sigma I} \quad . \qquad \text{A5}$$

The intensity I still has wavelength dependence, given by

$$I^{\lambda} = I_o{}^{\lambda} \exp(-\mu_m{}^{\lambda}{}_o \ell) \quad , \qquad \text{A6}$$

where $I_o{}^{\lambda}$ is the unattenuated intensity.

The shape of the intensity distribution is therefore dependent on the amount of absorption of the beam, through the $\exp(\rho\ell)$ function. This fact is unsettling when put in the perspective of a density diagnostic: the absorption coefficient is ambiguously related to the density measured. The nature and extent of this indeterminancy must be established. To analyze the mean absorption coefficient, a somewhat oversimplified intensity distribution is used. The major features of X-ray continuum distribution is a well-defined minimum wavelength (λ_{min} = 12400/V, where V is accelerating tube voltage), a peak at approximately $1.5\lambda_{min}$, and a λ^{-1} dependence at large wavelength (Reference 9). These major features are

incorporated in the simplified distribution shown in Figure A2a. The first curve is the intensity distribution with no absorption: the second curve is with absorption arising from $\rho\ell = 0.5$, and the third curve is with $\rho\ell = 5.0$. As the intensity curve shifts toward lower wavelength, the mean absorption coefficient should decrease, as shown by Figure A2b. The inherent absorption in the X-ray tube window is shown on this figure, along with experimental absorption data for talc. The absorption from the aluminum window greatly reduces the spread on effective absorption coefficient, with measured values varying from about 0.8 to 0.6.

The experimental absorption coefficients for talc were obtained by measuring attenuation of an X-ray beam through a known density and absorption length of talc powder. The standard deviation was 4% of the absorption coefficient value, as would be expected from the error analysis presented in a previous section.

Table 2 gives a short compilation of absorption coefficients for several powder materials that are of interest in portions of our multi-component flow investigations.

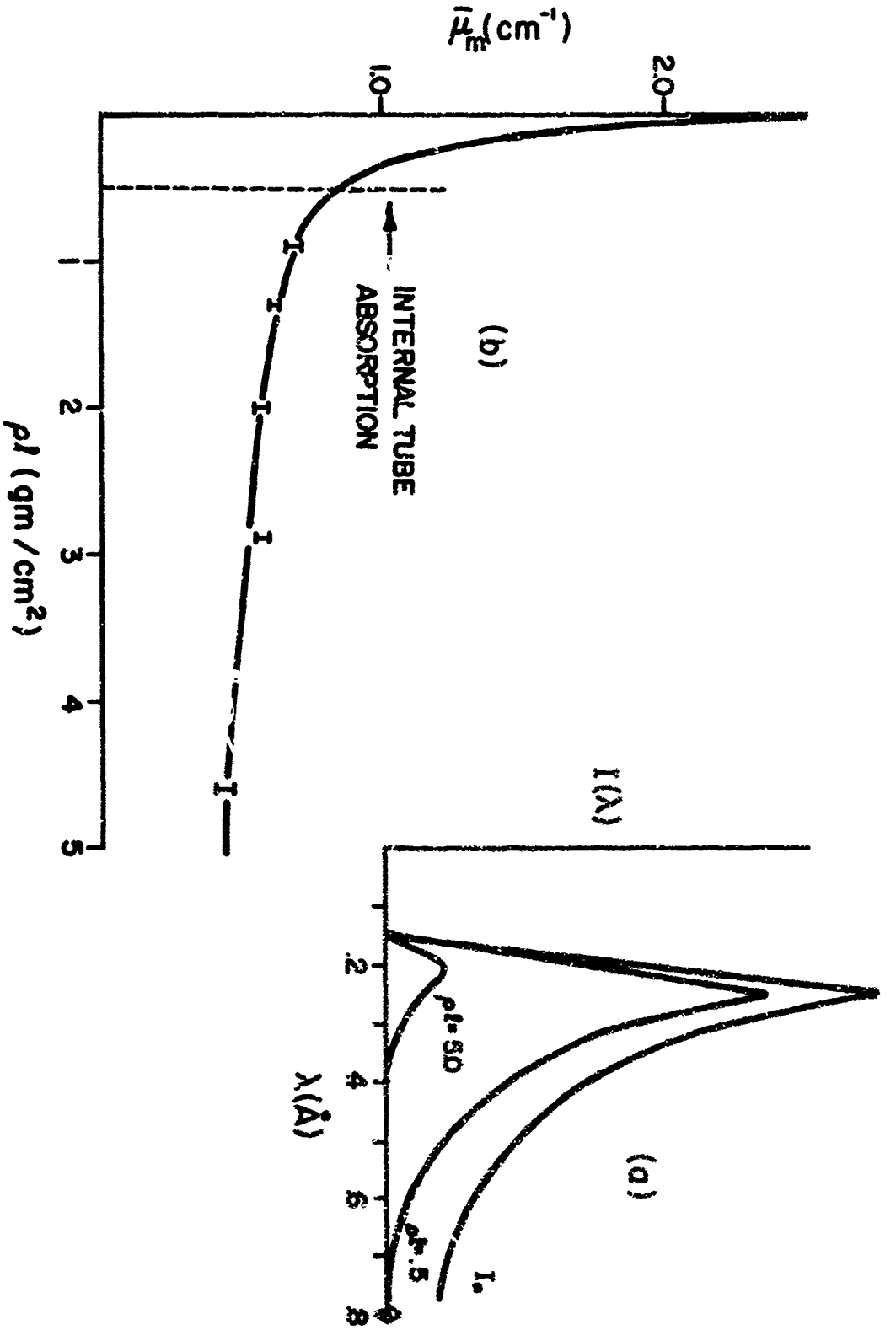

Fig. A2 Effect of Absorption Path Length on Effective Absorption Coefficient and Intensity Spectrum

Table 2

Mass Absorption Coefficients

Material	Composition	Density (gm/cm^3)	Mass Absorption Coefficient Calculated(0.26Å)	Experimental
Talc	$3MgO.SiO_2.H_2O$	2.73	0.31	.71
Aluminum Oxide	Al_2O_3	3.85	0.31	.55
Aluminum Powder Plasma Spray	Al	2.70	0.40	.90
Chromic Oxide	Cr_2O_3	5.21	1.33	1.46
Tungsten	W	19.	3.50	
Zinc	Zn	7.0	3.55	
Silica	SiO_2	2.20	.35	